Available online at www.sciencedirect.com
ScienceDirect
Trans. Nonferrous Met. Soc. China 30(2020) 1157−1168
Transactions of Nonferrous Metals Society of China
www.tnmsc.cn

Phase evolution in AlSi20/8009 aluminum alloy during high temperature heating near melting point and cooling processes

Hai-bin LIU[1], Hua-guang SU[2], Ding-fa FU[1], Fu-lin JIANG[1], Hui ZHANG[1]

1. College of Materials Science and Engineering, Hunan University, Changsha 410082, China;
2. Shanghai Electric Cable Research Institute Co., Ltd., Shanghai 200093, China

Received 29 September 2019; accepted 23 March 2020

Abstract: The AlSi20/8009 aluminum alloy was heated to high temperatures near the melting point and cooled to investigate the effect of external Si addition on the phase evolution of $Al_{12}(Fe,V)_3Si$ dispersion. Differential scanning calorimeter, scanning electron microscope, energy dispersive spectrometer and X-ray diffractometer were employed. The results showed that $Al_{12}(Fe,V)_3Si$ and Si phases evolved into a needle-like $Al_{4.5}FeSi$ phase and a nano-sized V-rich phase during holding the alloy at 580−600 °C. With increasing holding temperature to 620−640 °C, $Al_{4.5}FeSi$ and nano-sized V-rich phases evolved reversibly into $Al_{12}(Fe,V)_3Si$ and Si phases, of which $Al_{12}(Fe,V)_3Si$ occupied a coarse and hexagonal morphology. During the alloy (after holding at 640 °C) furnace cooling to 570 °C or lower, Si and $Al_{12}(Fe,V)_3Si$ phases evolved into strip-like $Al_{4.5}FeSi$ and the V-rich phases, which is a novel formation route for $Al_{4.5}FeSi$ phase different from Al−Fe−Si ternary system.

Key words: SiC_p/8009Al composite; phase evolution; metallurgical joining; re-melting; cooling

1 Introduction

The SiC particles reinforced 8009 aluminum matrix composite (SiC_p/8009Al composite) occupies light mass, good thermal stability, high elevated-temperature strength and high wear resistance and obtains a wide range of applications in the fields of automobile, aerospace and electronics [1−3]. However, SiC_p/8009Al composite also has a poor formability. To resolve the problem, it could be joined to casting aluminum alloys during fabricating complex parts such as pistons. Since the joining temperature was close to the melting point of the 8009 aluminum matrix, $Al_{12}(Fe,V)_3Si$ dispersions may be unstable and the formation of certain harmful intermetallic may occur. WHITAKER and McCARTNEY [4] studied the microstructure of CO_2 laser welding 8009 aluminum alloy and found that Al_mFe-type ($m\approx4$) precipitates appeared in the fusion zone. The study of HE et al [5] showed that $Al_{12}(Fe,V)_3Si$ dispersions in 8009 aluminum alloy were transformed into θ-$Al_{13}Fe_4$ and h-AlFeSi phases after being exposed at 600 °C for 10 h. The work of SUN et al [6] showed that when the selective laser melting 8009 aluminum alloy was hold at 600 °C for 100 h, $Al_{13}Fe_4$ and Al_8Fe_2Si phases were formed by consuming $Al_{12}(Fe,V)_3Si$ dispersions. As is known, $Al_{12}(Fe,V)_3Si$ is a nanoscale phase

Foundation item: Project (CX20190310) supported by the Hunan Provincial Innovation Foundation for Postgraduate, China; Project (51574118) supported by the National Natural Science Foundation of China; Project (2016GK4056) supported by Key Technologies R & D in Strategic Emerging Industries and Transformation in High-tech Achievements Program of Hunan Province, China; Project (2018GK5068) supported by Innovation and Entrepreneurship Technology Investment Project of Hunan Province, China

Corresponding author: Ding-fa FU, Tel: +86-731-88664086, Fax: +86-731-88821483, E-mail: hunu_fudingfa@163.com;
Hui ZHANG, Tel: +86-731-88664086, Fax: +86-731-88821483, E-mail: zhanghui63hunu@163.com, zhanghui63@hnu.edu.cn

DOI: 10.1016/S1003-6326(20)65286-4

supporting good thermally mechanical properties of 8009 aluminum alloy and its composites [7−9]. Thus, the phase evolution of $Al_{12}(Fe,V)_3Si$ dispersions is undesirable and should be avoided.

In our recent study [10], SiC_p/8009Al composite and A356 aluminum alloy were joined together using compound casting. However, a large amount of strip-like $Al_{4.5}FeSi$ phases were formed in the transition zone. As is known, $Al_{4.5}FeSi$ phase is detrimental to the mechanical properties and workability of aluminum alloys due to its sharp needle-like shape [11−13]. It was deduced that the Si element of A356 aluminum alloy melt diffusing into the melted SiC_p/8009Al composite should be responsible for the formation of $Al_{4.5}FeSi$ phase. To confirm the inference, an investigation program was designed [14], where AlSi20 alloy powders and rapidly solidified 8009 aluminum alloy powders were mixed and extruded into an AlSi20/8009 aluminum alloy. The AlSi20/8009 aluminum alloy was then annealed at 480−540 °C and the results proved that the external Si addition could result in the dissolution of some $Al_{12}(Fe,V)_3Si$ dispersions and the formation of needle-like $Al_{4.5}FeSi$ and nano-sized V-rich phases. However, the above annealing treatments could not melt the 8009 aluminum matrix. Therefore, the formation and cooling processes of the transition zone during compound casting or other solid−liquid joining processes could not be fully simulated. In addition, the $Al_{4.5}FeSi$ phase formed during compound casting occupying a strip-like rather than a needle-like shape also required further explanation.

Therefore, in the present study, the as-extruded AlSi20/8009 aluminum alloy was heated to high temperatures near the melting point. The phase evolution during heating and cooling processes of the AlSi20/8009 aluminum alloy was comprehensively studied by comparing with the 8009 aluminum alloy. The effect of cooling conditions on the phase evolution in the AlSi20/8009 aluminum alloy was also investigated. Finally, the phase evolution route was discussed and the change in morphology of $Al_{4.5}FeSi$ phase was explained.

2 Experimental

The rapidly solidified 8009 aluminum alloy powders, which had the main chemical composition of 9.0 wt.% Fe, 1.19 wt.% V and 2.22 wt.% Si, and 21.6 wt.% AlSi20 alloy powders were used to prepare the AlSi20/8009 aluminum alloy. The preparation procedure containing powder mixing, canning, vacuum degassing, densification and extrusion was illustrated in detail in our previous work [14]. As a contrast, the 8009 aluminum alloy was prepared utilizing the same process without adding the AlSi20 alloy powders.

As shown in Fig. 1, the AlSi20/8009 aluminum alloy samples were heated to 580−640 °C, held for 10 min and then water-quenched to investigate the phase evolution during heating process. The 8009 aluminum alloy experienced the same treatment to investigate the role of external Si addition in the phase evolution of the AlSi20/8009 aluminum alloy. To investigate the phase evolution during cooling process, the AlSi20/8009 aluminum alloy samples were held at 640 °C for 10 min, furnace cooled to 615−560 °C and then water quenched. The effect of cooling rate on the phase evolution in the AlSi20/8009 aluminum alloy was investigated using the following process. The AlSi20/8009 aluminum alloy samples were held at 640 °C for 10 min, furnace- or air-cooled to 555 °C and then water-quenched. All the samples were cut into *d*17 mm × 15 mm cylinders from the extruded rods using wire electrical discharge machining (WEDM).

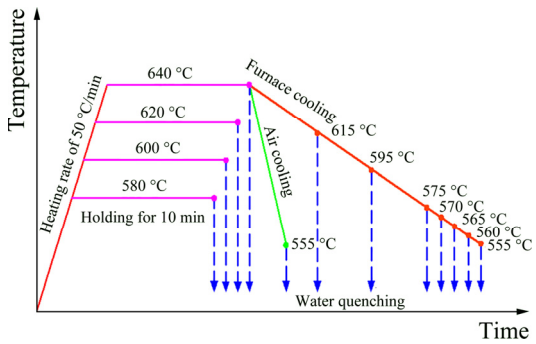

Fig. 1 Schematic description of heating and cooling processes

A NETZSCH STA 449C differential scanning calorimeter (DSC) was used to measure the starting melting and solidification points of the as-extruded AlSi20/8009 and 8009 aluminum alloys. A heating rate of 10 K/min and a cooling rate of 10 K/min were applied in the temperature interval of 500−700 °C. A ZEISS EVO MA10 scanning electron microscope (SEM) was used to observe the

microstructures of experimental samples. An Oxford energy dispersive spectrometer (EDS) equipped on the SEM was used to measure the chemical composition of different phases. At least six points were measured for each phase. A Rigaku D/Max 2500 X-ray diffractometer (XRD) was used for the phase identification of experimental samples. A Cu target at 40 kV and 250 mA was used and diffraction patterns in the 2θ range of 10°−90° were recorded at a scanning speed of 8 (°)/min. All the samples for above examinations were sectioned from the planes parallel to the extrusion direction.

3 Results

3.1 DSC curves of as-extruded AlSi20/8009 and 8009 aluminum alloys

Figures 2(a) and (b) show the DSC curves of the as-extruded 8009 aluminum alloy and AlSi20/8009 aluminum alloy, respectively. It is observed that the starting melting point and the starting solidification point of the as-extruded 8009 aluminum alloy are 628.5 and 631.5 °C, respectively. In contrast, there are two peaks present in ether heating or cooling process of the as-extruded AlSi20/8009 aluminum alloy. The first starting melting point of the as-extruded AlSi20/8009 aluminum alloy is 571.2 °C, which is close to the eutectic point of Al−Si alloy. It has been shown that the external Si formed Si-rich strips and blocks in the as-extruded AlSi20/8009 aluminum alloy [14]. Therefore, the Al−Si eutectic of the as-extruded AlSi20/8009 aluminum alloy is melted first during the heating process. Then, the second stage of the melting is activated without an intermittent due to the diffusion of Si element into the 8009 aluminum matrix. During the cooling process, the first starting solidification point of the as-extruded AlSi20/8009 aluminum alloy is 617.4 °C. Similar to the heating process, there is no obvious intermittent between the first and second solidification stages due to the ejection of Si element from the 8009 aluminum matrix. Therefore, according to the DSC results shown in Fig. 2, there is liquid alloy present in the 8009 aluminum alloy during holding at 640 °C, while the 8009 aluminum matrix of the AlSi20/8009 aluminum alloy is gradually melted after the Al−Si eutectic melting is completed. Meanwhile, it is expected that the 8009 aluminum matrix of the AlSi20/8009 aluminum alloy is melted more drastically when holding at 620 and 640 °C.

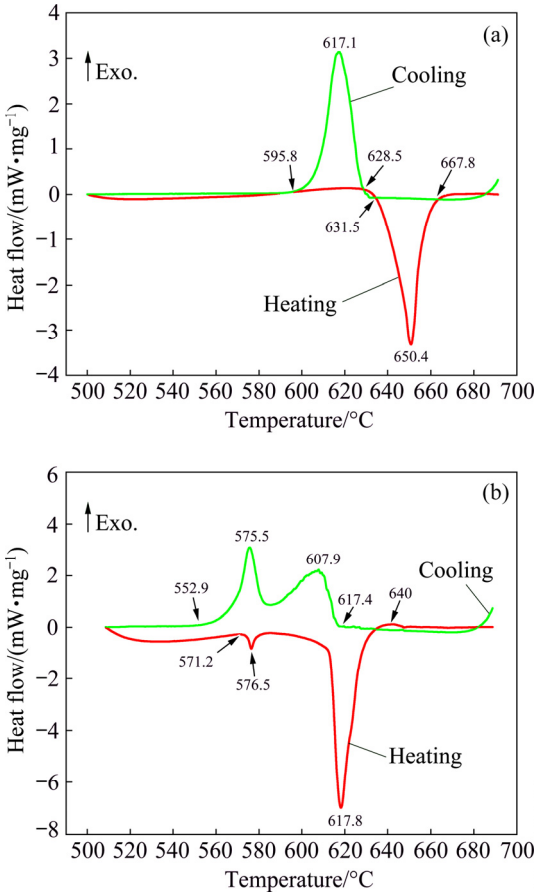

Fig. 2 DSC curves of as-extruded 8009 (a) and AlSi20/8009 (b) aluminum alloys

3.2 Phase evolution in AlSi20/8009 aluminum alloy during heating process

Figure 3 shows the microstructures of the AlSi20/8009 aluminum alloy samples after holding at different temperatures for the same time of 10 min. As shown in Figs. 3(a) and (b), the microstructures of the samples after holding at 580 and 600 °C are similar to that after annealing at 540 °C (as shown in Ref. [14]). Vast number of needle-like $Al_{4.5}FeSi$ phases are formed while $Al_{12}(Fe,V)_3Si$ and Si phases are decreased in their contents, as shown in Fig. 3(e). With increasing holding temperature to 620 °C, the density of $Al_{4.5}FeSi$ phase is decreased and many coarse and hexagonal $Al_{12}(Fe,V)_3Si$ phases are present in Fig. 3(c). Further increasing holding temperature to 640 °C, as shown in Fig. 3(d), needle-like $Al_{4.5}FeSi$ phase disappears and only the coarse and hexagonal $Al_{12}(Fe,V)_3Si$ phase can be observed. The XRD

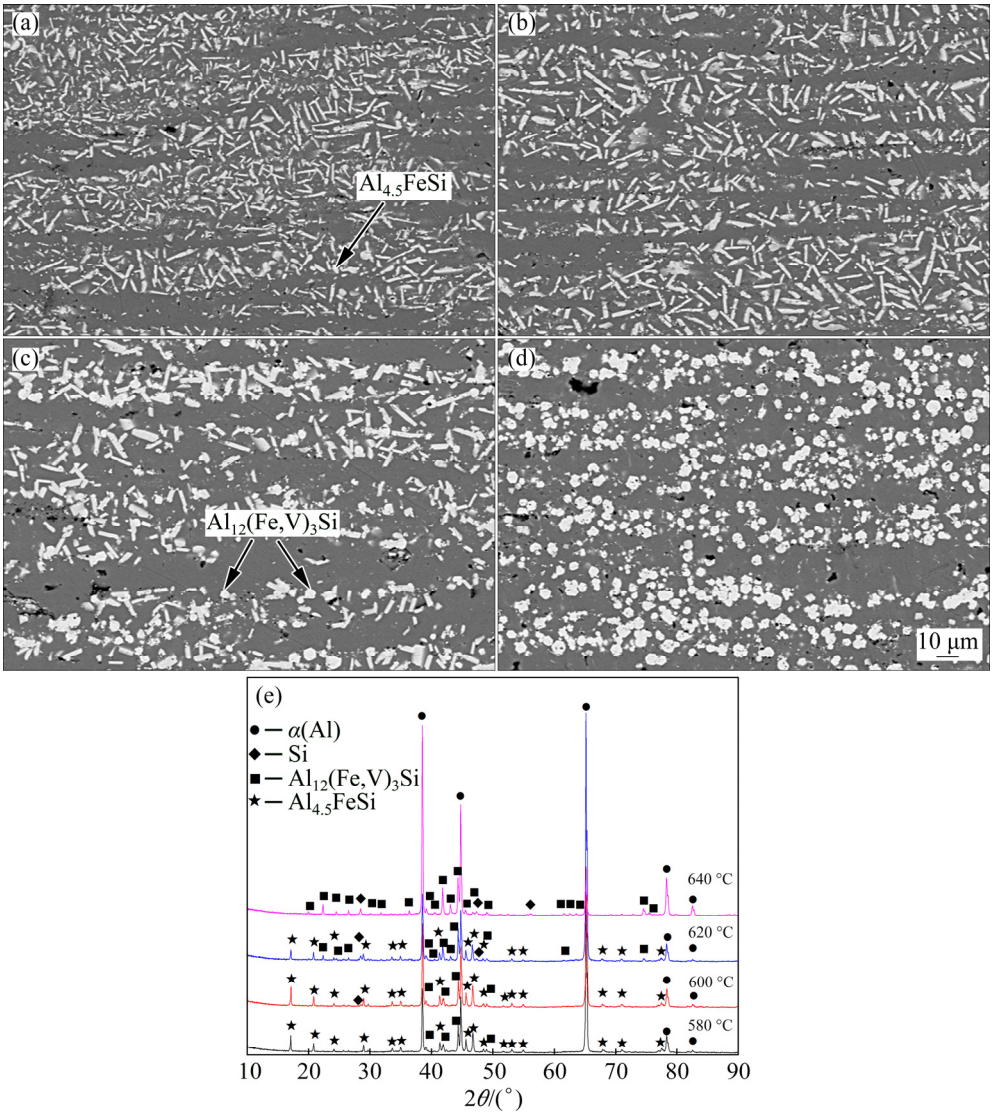

Fig. 3 SEM micrographs (a−d) and XRD patterns (e) of AlSi20/8009 aluminum alloy samples after holding for 10 min at 580 °C (a), 600 °C (b), 620 °C (c) and 640 °C (d)

patterns in Fig. 3(e) validate the above observations at the holding temperatures of 620 and 640 °C. The gradually disappeared peaks of $Al_{4.5}FeSi$ phase reflect its decreased content, while the strengthened peaks of $Al_{12}(Fe,V)_3Si$ and Si phases indicate their increased contents.

Figure 4(a) shows a high magnification SEM micrograph of the AlSi20/8009 aluminum alloy sample after holding at 620 °C for 10 min. The nano-sized V-rich phases with granular shape and bright color, which appeared in our previous work [14], can be still observed. Combined with the XRD patterns in Fig. 3(e), the EDS result in Fig. 4(c) proves that the coarse and hexagonal phase shown in Fig. 4(a) is $Al_{12}(Fe,V)_3Si$ phase. Figure 4(b) shows a high magnification SEM micrograph of the AlSi20/8009 aluminum alloy sample after holding at 640 °C for 10 min. The EDS result in Fig. 4(d) proves that the Si-rich regions distribute around the voids. Compared with the 8009 aluminum matrix, the Si-rich regions occupy a slightly brighter contrast. As can be seen, the Si phase did not form coarse grains. This is due to the following factors. One is the preparation method of rapid solidification for the AlSi20 alloy powders, the other is suddenly water quenching during holding the AlSi20/8009 aluminum alloy at high temperatures. Due to the fine grain characteristic of Si phase, no obvious trends of density of Si phase can be observed in Figs. 3(a−d). During heating process, as mentioned above, Al−Si eutectic was melted and a part of Si in Si-rich blocks diffused

into the 8009 aluminum matrix, which resulted in the formation of voids.

3.3 Microstructures of 8009 aluminum alloy after holding at high temperatures

As a contrast, the as-extruded 8009 aluminum alloy samples were also held for 10 min at 580−640 °C. As can be observed in Fig. 5, the microstructures of the 8009 aluminum alloy samples maintained stable with increasing the holding temperature. The streamlines and powder particles appearing in the as-extruded 8009

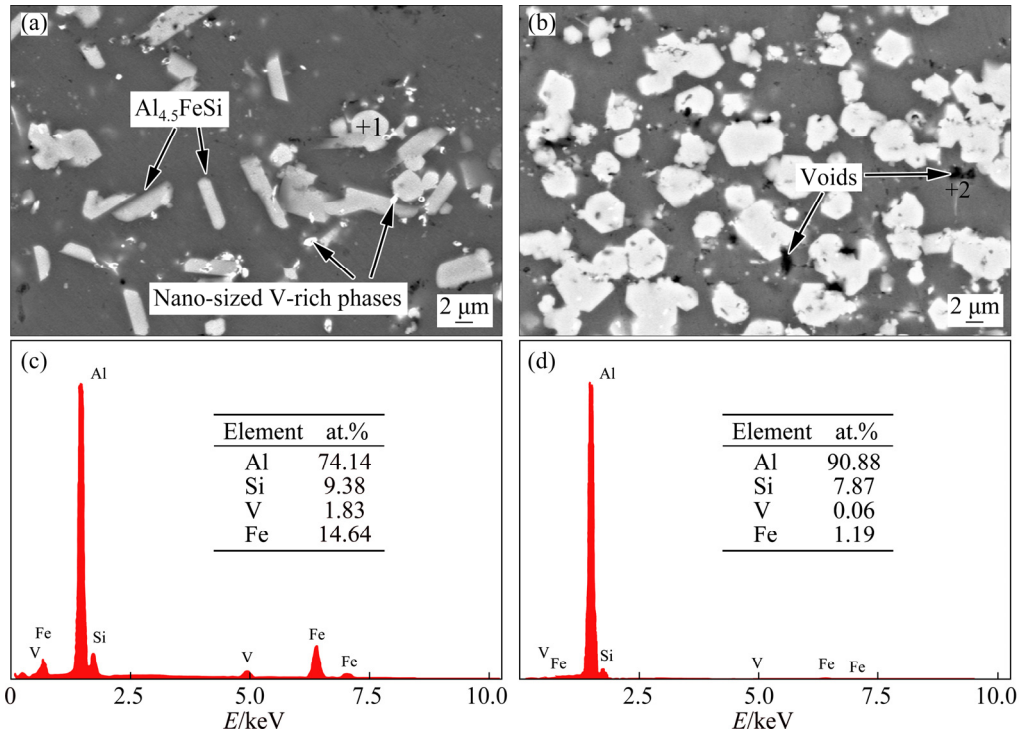

Fig. 4 High magnification SEM micrographs (a, b) and EDS results (c, d) of AlSi20/8009 aluminum alloy samples after holding for 10 min: (a) 620 °C; (b) 640 °C; (c) Point 1 in Fig. 4(a); (d) Point 2 in Fig. 4(b)

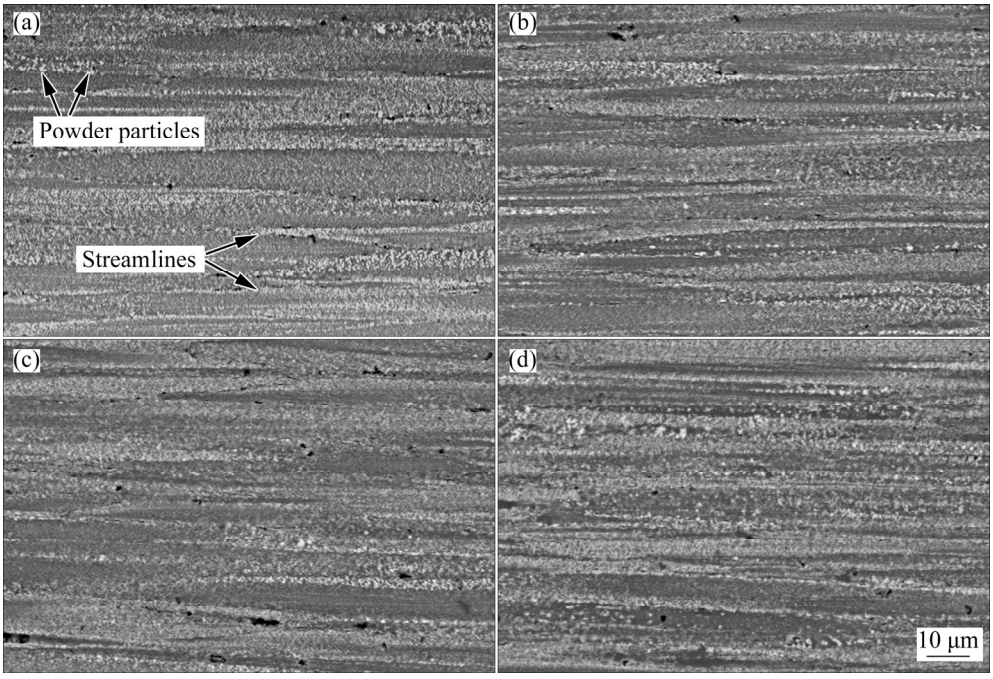

Fig. 5 SEM micrographs of 8009 aluminum alloy samples after holding for 10 min at 580 °C (a), 600 °C (b), 620 °C (c) and 640 °C (d)

aluminum alloy [14] were retained in the annealed 8009 aluminum alloy samples. In other words, as compared with the AlSi20/8009 aluminum alloy samples, no similar phase evolution occurred in the 8009 aluminum alloy samples during holding at high temperatures.

3.4 Phase evolution in AlSi20/8009 aluminum alloy during cooling process

Figure 6 shows the microstructures of the AlSi20/8009 aluminum alloy samples after holding at 640 °C for 10 min and then furnace cooling from 640 to 575 °C. The microstructures maintained stable when decreasing the target temperatures of furnace cooling. The XRD results in Fig. 6(e) were consistent with above observations. Therefore, no phase evolution occurred during the cooling process of the AlSi20/8009 aluminum alloy samples.

Figures 7(a−d) show high magnification SEM micrographs of the AlSi20/8009 aluminum alloy samples after holding at 640 °C for 10 min and then furnace cooling from 640 to 575 °C. When the target temperatures of furnace cooling are 640−595 °C, as shown in Figs. 7(a−c), only the coarse and hexagonal $Al_{12}(Fe,V)_3Si$ phases are observed. However, with decreasing the target temperature of furnace cooling to 575 °C, as shown in Fig. 7(d), a few fine needle-like $Al_{4.5}FeSi$ phases are formed near the coarse and hexagonal $Al_{12}(Fe,V)_3Si$ phases. It is worth noticing that the growth orientation of $Al_{4.5}FeSi$ phase is random. The nano-sized V-rich phases can also be identified

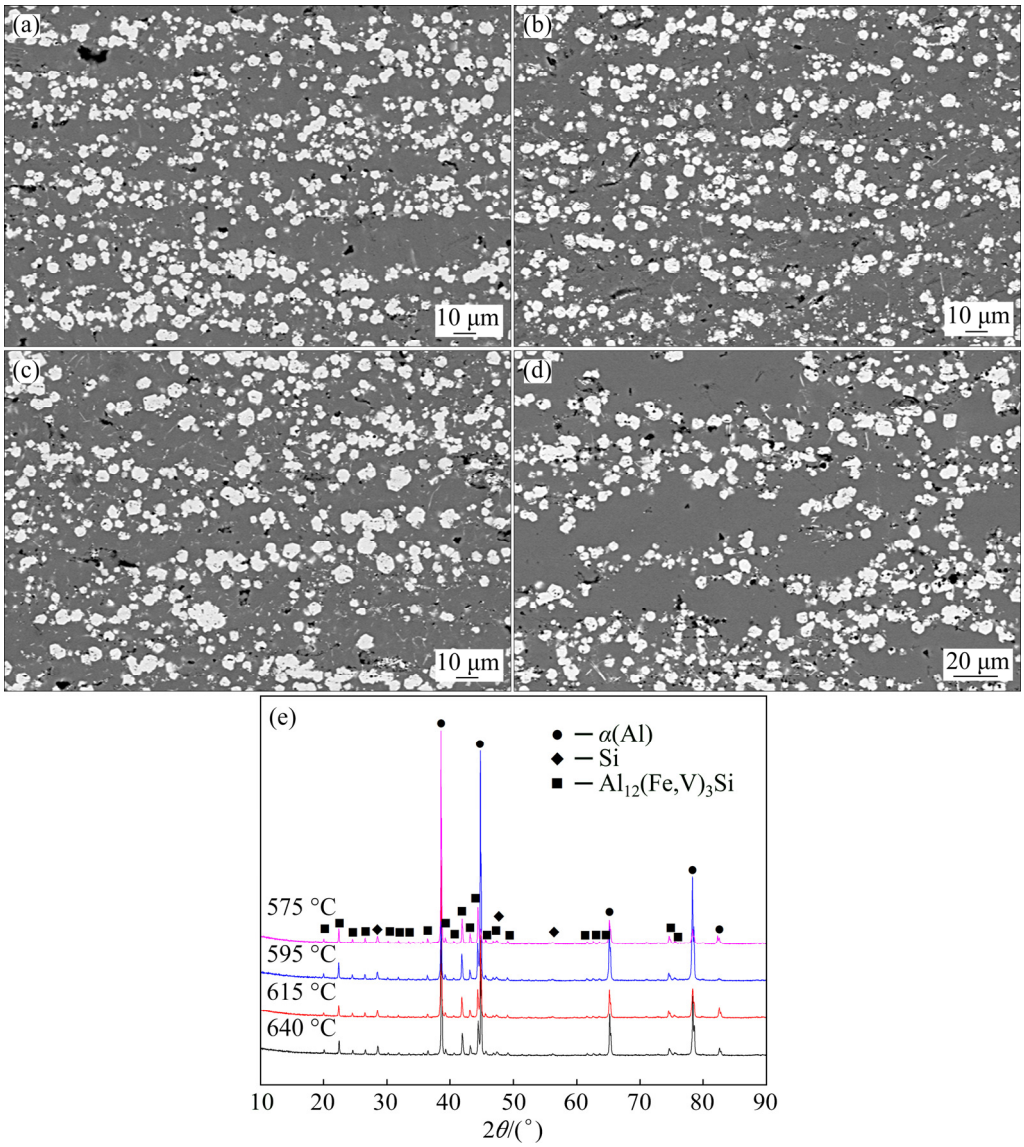

Fig. 6 SEM micrographs (a−d) and XRD patterns (e) of AlSi20/8009 aluminum alloy samples after holding at 640 °C for 10 min and then furnace cooling to 640 °C (a), 615 °C (b), 595 °C (c) and 575 °C (d)

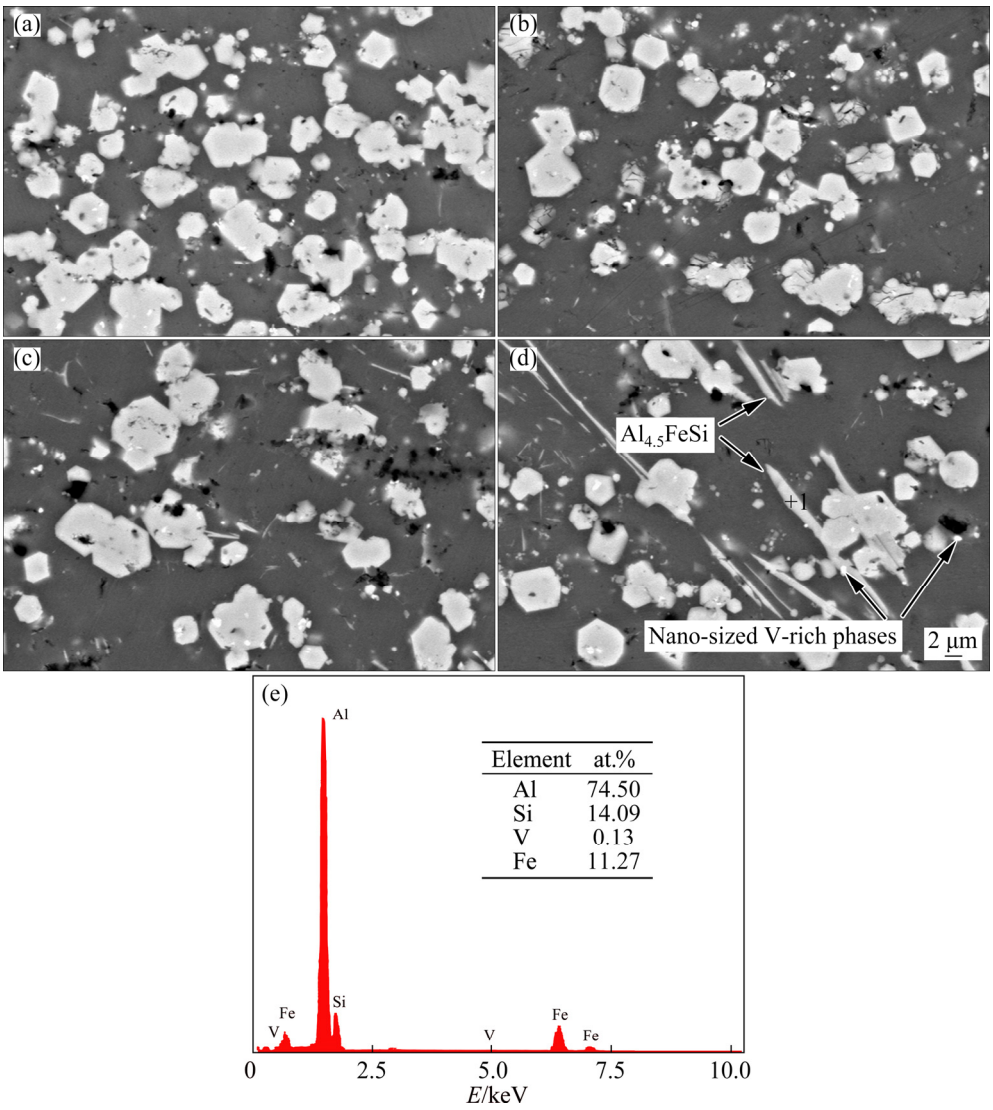

Fig. 7 High magnification SEM micrographs of AlSi20/8009 aluminum alloy samples after holding at 640 °C for 10 min and then furnace cooling to 640 °C (a), 615 °C (b), 595 °C (c) and 575 °C (d) and EDS result of Point 1 in Fig. 7(d) (e)

due to their granular shape and brighter contrast. The EDS result in Fig. 7(e) proves that the needle-like phase is $Al_{4.5}FeSi$. The excessive V element should come from the 8009 aluminum matrix since the needle-like $Al_{4.5}FeSi$ phase is too fine.

Figure 8 shows the microstructures and XRD patterns of the AlSi20/8009 aluminum alloy samples after holding at 640 °C for 10 min and then furnace cooling from 570 to 560 °C. When the target temperature of furnace cooling decreases to 570 °C, as shown in Figs. 8(a) and (d), $Al_{4.5}FeSi$ phase is formed obviously. Further decreasing the target temperature of furnace cooling to 560 °C, the density of $Al_{4.5}FeSi$ phase is intensively increased while that of the coarse and hexagonal $Al_{12}(Fe,V)_3Si$ phase shows an opposite trend, as shown in Fig. 8(c). The weakened peaks of Si phase imply its decreased content, as shown in Fig. 8(d). Meanwhile, it is worth noticing that the formed $Al_{4.5}FeSi$ phase occupies a strip-like rather than needle-like shape.

Figure 9 shows high magnification SEM micrographs of the AlSi20/8009 aluminum alloy samples after holding at 640 °C for 10 min and then furnace cooling to 570 and 560 °C. When the target temperature of furnace cooling is 570 °C, the coarse and hexagonal $Al_{12}(Fe,V)_3Si$ phase can be clearly identified, as remarked by the red line in Fig. 9(a). And the formed $Al_{4.5}FeSi$ phase tends to surround

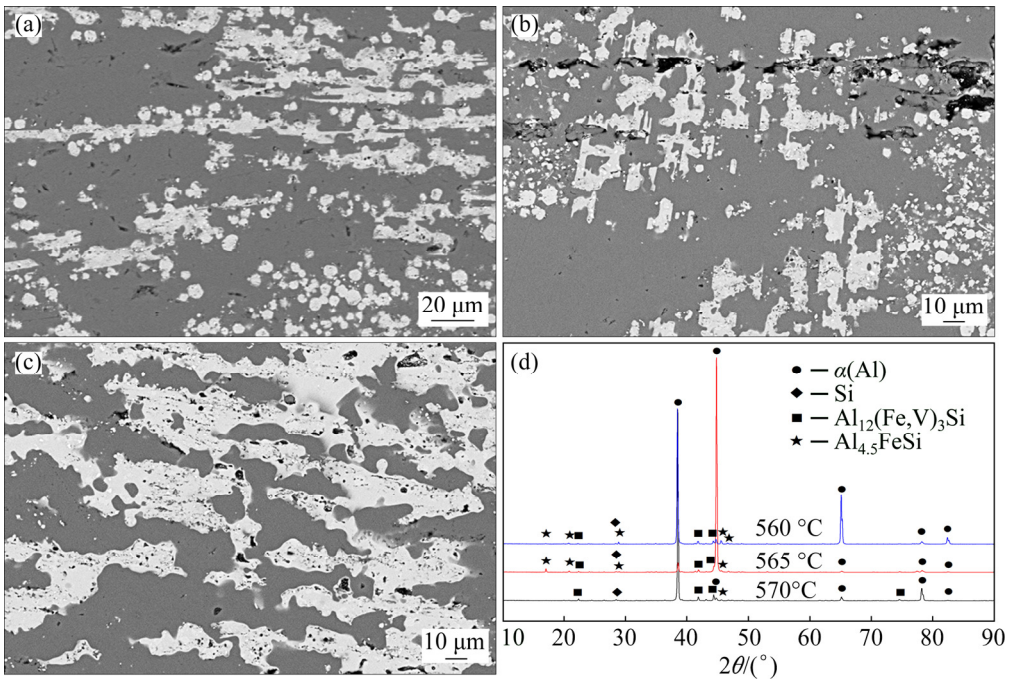

Fig. 8 SEM micrographs (a−c) and XRD patterns (d) of AlSi20/8009 aluminum alloy samples after holding at 640 °C for 10 min and then furnace cooling to 570 °C (a), 565 °C (b) and 560 °C (c)

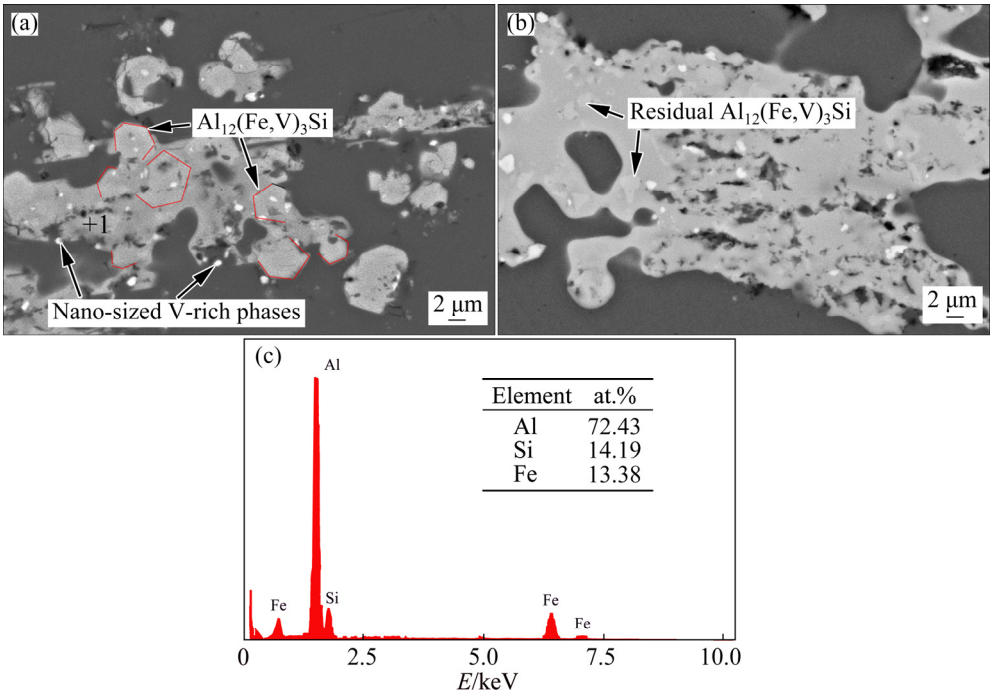

Fig. 9 High magnification SEM micrographs of AlSi20/8009 aluminum alloy samples after holding at 640 °C for 10 min and then furnace cooling to 570 °C (a) and 560 °C (b) and EDS result of Point 1 in Fig. 9(a) (c)

the $Al_{12}(Fe,V)_3Si$ phases. However, with decreasing the target temperature of furnace cooling to 560 °C, only residual $Al_{12}(Fe,V)_3Si$ phase can be observed and the growth of $Al_{4.5}FeSi$ phase occurs, as shown in Fig. 9(b). In addition, vast number of the nano-sized V-rich phases can be observed in Figs. 9(a) and (b). The EDS result in Fig. 9(c) and the XRD patterns in Fig. 8(d) confirm that the strip-like phase shown in Fig. 9(a) is $Al_{4.5}FeSi$ phase.

Figures 10(a, b) show the microstructures of the AlSi20/8009 alloy samples after holding at 640 °C for 10 min and then cooling to 555 °C with furnace and air. The XRD patterns shown in Fig. 10(c) prove that the phase identification has no obvious difference between the above two cooling conditions. However, as compared with furnace cooling, $Al_{4.5}FeSi$ phase formed under air cooling has a finer morphology.

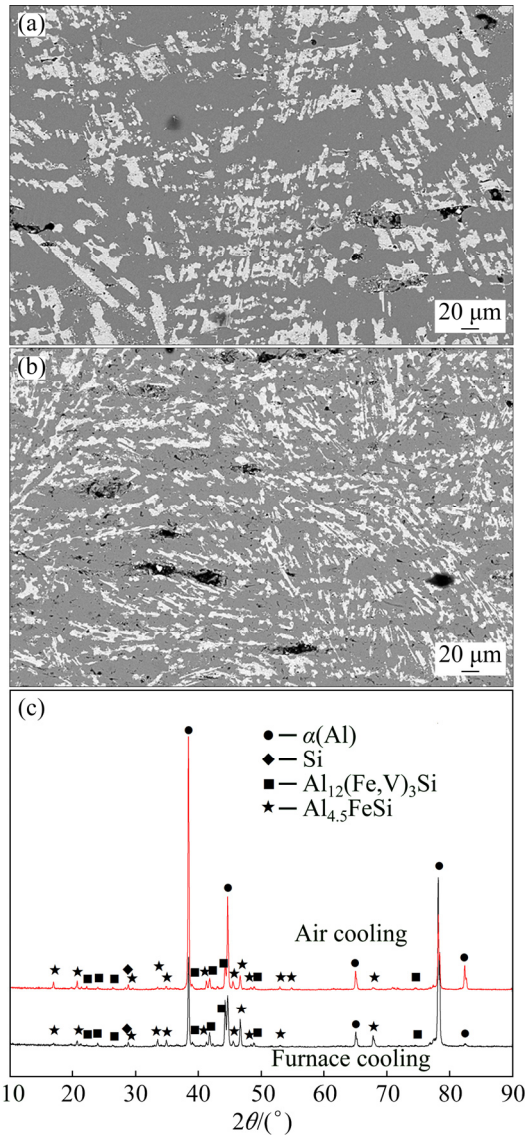

Fig. 10 SEM micrographs of AlSi20/8009 alloy samples after holding at 640 °C for 10 min and then furnace cooling (a) and air cooling (b) to 555 °C and XRD patterns (c)

4 Discussion

$Al_{12}(Fe,V)_3Si$ dispersion could evolve into other phases under certain conditions, as proved by previous studies [4−6,14]. When the AlSi20/8009 aluminum alloys were held for 10 min at 580 and 600 °C, as shown in Figs. 3(a) and (b), similar microstructures as annealed at 540 °C were obtained. According to literature [14], the formation of needle-like $Al_{4.5}FeSi$ and the nano-sized V-rich phases was attributed to the consumption of $Al_{12}(Fe,V)_3Si$ dispersions and the external Si addition. With increasing holding temperature to 620 and 640 °C, the 8009 aluminum matrix of the AlSi20/8009 aluminum alloy was drastically melted (Fig. 2(b)). As shown in Figs. 3(c) and (d), the content of $Al_{4.5}FeSi$ phase was gradually decreased while that of $Al_{12}(Fe,V)_3Si$ and Si phases showed an opposite trend. It was indicated that the phase evolution, where $Al_{12}(Fe,V)_3Si$ and Si phases were consumed to form $Al_{4.5}FeSi$ and the nano-sized V-rich phases, was a reversible process. $Al_{4.5}FeSi$ and nano-sized V-rich phases lost their thermodynamic stability and free Fe and V elements were released. Meanwhile, the coarsening of previously stable $Al_{12}(Fe,V)_3Si$ dispersions was activated and free Fe and V elements were consumed. The results in Ref. [4] proved that once the 8009 aluminum matrix was melted without the external Si addition, $Al_{12}(Fe,V)_3Si$ dispersions would evolve into Al−Fe binary intermetallic. Combined with the stable microstructures of the 8009 aluminum alloy in Fig. 5, it was proved that the reversible phase evolution process required the participation of the external Si element.

When the AlSi20/8009 aluminum alloy was held at 640 °C for 10 min and then furnace-cooled to 575 °C, the phase evolution route was different from that of Al−Fe−Si ternary system. As shown in Refs. [15−18], the reactions for the formation of $Al_{4.5}FeSi$ phase can be listed as follows:

$$L \rightarrow \text{Al dendritic network (655 °C)} \quad (1)$$

$$L \rightarrow Al + Al_8Fe_2Si \text{ (615−618 °C)} \quad (2)$$

$$L + Al_8Fe_2Si \rightarrow L + Al_{4.5}FeSi \text{ (610 °C)} \quad (3)$$

$$L \rightarrow Al + Al_{4.5}FeSi + Si \text{ (576 °C)} \quad (4)$$

As proved by Figs. 7 and 8, there was no Chinese script-like Al_8Fe_2Si phase [19−23] formed during the furnace cooling process of the AlSi20/8009 aluminum alloy after 640 °C holding. Previous literatures [24] and [25] showed that larger cooling rate could suppress the formation of

$Al_{4.5}FeSi$ phase and promote the formation of Al_8Fe_2Si phase. However, as shown in Fig. 10, no Al_8Fe_2Si phase was formed and only $Al_{4.5}FeSi$ phase became finer even under air cooling condition. In other words, the phase evolution route of Al−Fe−Si ternary system could not apply to the cooling process of the AlSi20/8009 aluminum alloy after 640 °C holding. As shown in Figs. 8 and 9, the formation and growth of $Al_{4.5}FeSi$ and nano-sized V-rich phases were attributed to the consumption of $Al_{12}(Fe,V)_3Si$ and Si phases. Therefore, it can be concluded that, during the above mentioned cooling process, $Al_{12}(Fe,V)_3Si$ and Si phases were directly evolved into $Al_{4.5}FeSi$ and nano-sized V-rich phases, with no Al_8Fe_2Si as a transition phase.

As shown in Figs. 3 and 8, whether in the AlSi20/8009 aluminum alloy samples after holding at 580−600 °C or in the AlSi20/8009 aluminum alloy samples after holding at 640 °C and then furnace cooling to 570−560 °C, $Al_{4.5}FeSi$ phases were formed. However, the formed $Al_{4.5}FeSi$ phases showed different morphologies. One occupied a needle-like shape, the other had a strip-like shape. This may be due to their different nucleation and growth conditions. When the AlSi20/8009 aluminum alloy samples were annealed at 580−600 °C, the 8009 aluminum matrix maintained fine microstructure with a grain size of about 300 nm[14]. A large number of grain boundaries could serve as nucleation sites and elemental diffusion channels for $Al_{4.5}FeSi$ phases. Vast number of $Al_{4.5}FeSi$ phases could simultaneously nucleate and grow, and absorb nearby free Al, Fe and Si atoms. Therefore, different $Al_{4.5}FeSi$ phases could grow independently and occupy a needle-like shape. In contrast, the 8009 aluminum matrix of the AlSi20/8009 aluminum alloy samples was drastically melted after holding at 640 °C for 10 min. $Al_{4.5}FeSi$ phases tended to nucleate near the coarse and hexagonal $Al_{12}(Fe,V)_3Si$ phases, as shown in Fig. 7(d). To reduce the diffusion distance of atoms and the energy barrier of phase evolution, as shown in Fig. 9, $Al_{4.5}FeSi$ phases tended to surround the coarse and hexagonal $Al_{12}(Fe,V)_3Si$ phases and then gradually consume the coarse and hexagonal $Al_{12}(Fe,V)_3Si$ phases for growth. In other words, the distribution of the coarse and hexagonal $Al_{12}(Fe,V)_3Si$ phases may constrain the final shape of $Al_{4.5}FeSi$ phases. Meanwhile, considering the fact that the growth orientation of $Al_{4.5}FeSi$ phases was random, different $Al_{4.5}FeSi$ phases tended to cross and aggregate to form a strip-like shape. When the cooling rate of solidification process was larger, as shown in Fig. 10(b), there was a shorter period for the growth and aggregation of $Al_{4.5}FeSi$ phases. Thus, $Al_{4.5}FeSi$ phase formed under air cooling condition occupied a finer morphology.

5 Conclusions

(1) When the AlSi20/8009 aluminum alloy was held for 10 min at 580−600 °C, needle-like $Al_{4.5}FeSi$ and nano-sized V-rich phases were formed by consuming $Al_{12}(Fe,V)_3Si$ dispersions and Si phase. With increasing holding temperature to 620−640 °C, the contents of Si and coarse and hexagonal $Al_{12}(Fe,V)_3Si$ phases increased by consuming $Al_{4.5}FeSi$ and nano-sized V-rich phases. It was proved that the phase evolution during heating the AlSi20/8009 aluminum alloy to 640 °C was a reversible process.

(2) When the AlSi20/8009 aluminum alloy was held at 640 °C and then furnace-cooled to 575 °C, the microstructure maintained stable. Further furnace cooling to 570 and 560 °C, $Al_{4.5}FeSi$ and nano-sized V-rich phases were formed by consuming the coarse and hexagonal $Al_{12}(Fe,V)_3Si$ and Si phases. Meanwhile, the formed $Al_{4.5}FeSi$ phase during furnace cooling showed a strip-like rather than needle-like shape.

(3) As compared with furnace cooling to 555 °C, the AlSi20/8009 aluminum alloy after holding at 640 °C and then air cooling to 555 °C had similar phase identification but a finer morphology of $Al_{4.5}FeSi$ phase. It was proved that a novel formation route of $Al_{4.5}FeSi$ phase was found, which was different from Al−Fe−Si ternary system.

References

[1] MA Z Y, TONG S C. High temperature creep behavior of SiC particulate reinforced Al−Fe−V−Si alloy composite [J]. Materials Science and Engineering A, 2000, 278: 5−15.

[2] CHEN Zhen-hua, HE Yi-qiang, YAN Hong-ge, CHEN Zhi-gang, YIN Xian-jue, CHEN Gang. Ambient temperature mechanical properties of Al−8.5Fe−1.3V−1.7Si/SiC_p composite [J]. Materials Science and Engineering A, 2007, 460−461: 180−185.

[3] CHEN Shuang, TENG Jie, LUO Hai-bo, WANG Yu, ZHANG Hui. Hot deformation characteristics and mechanism of PM 8009Al/SiC particle reinforced

composites [J]. Materials Science and Engineering A, 2017, 697: 194−202.

[4] WHITAKER I R, McCARTNEY D G. The microstructure of CO_2 laser welds in an Al−Fe−V−Si alloy [J]. Materials Science and Engineering A, 1995, 196: 155−163.

[5] HE Yi-qiang, QIAO Bin, WANG Na, YANG Jian-ming, XU Zheng-kun, CHEN Zhen-hua, CHEN Zhi-gang. Thermostability of monolithic and reinforced Al−Fe−V−Si materials [J]. Advanced Composite Materials, 2009, 18: 339−350.

[6] SUN Shao-bo, ZHENG Li-jing, LIU Jin-hui, ZHANG Hu. Selective laser melting of an Al−Fe−V−Si alloy: Microstructural evolution and thermal stability [J]. Journal of Materials Science & Technology, 2017, 33: 389−396.

[7] SKINNER D J, BYE R L, RAYBOULD D, BROWN A M. Dispersion strengthened Al−Fe−V−Si alloys [J]. Scripta Metallurgica, 1986, 20: 867−872.

[8] TANG Jin-jun, FEI Liang-jun, GONG Zhao-hui, ZHU Xiu-rong, SHI Hong-xia. Effect of alloy composition on the microstructure and mechanical properties of Al−Fe−V−Si heat-resistant aluminum alloy [J]. Applied Mechanics and Materials, 2013, 433−435: 2072−2075.

[9] SUN Shao-bo, ZHENG Li-jing, PENG Hui, ZHANG Hu. Microstructure and mechanical properties of Al−Fe−V−Si aluminum alloy produced by electron beam melting [J]. Materials Science and Engineering A, 2016, 659: 207−214.

[10] LIU Hai-bin, FU Ding-fa, DONG Zhao-yu, HUANG Shao-xiong, ZHANG Hui. Bonding interfacial characterization of SiC_p/8009Al composite and A356 aluminum alloy using compound casting [J]. Journal of Materials Processing Technology, 2019, 263: 42−49.

[11] MOUSTAFA M A. Effect of iron content on the formation of β-Al_5FeSi and porosity in Al−Si eutectic alloys [J]. Journal of Materials Processing Technology, 2009, 209: 605−610.

[12] TERZI S, TAYLOR J A, CHO Y H, SALVO L, SUÉRY M, BOLLER E, DAHLE A K. In situ study of nucleation and growth of the irregular α-Al/β-Al_5FeSi eutectic by 3-D synchrotron X-ray microtomography [J]. Acta Materialia, 2010, 58: 5370−5380.

[13] PEREIRA L H, ASATO G H, OTANI L B, JORGE A M Jr, KIMINAMI C S, BOLFARINI C, BOTTA W J. Changing the solidification sequence and the morphology of iron-containing intermetallic phases in AA6061 aluminum alloy processed by spray forming [J]. Materials Characterization, 2018, 145: 507−515.

[14] LIU Hai-bin, ZHANG Hui, JIANG Fu-lin, FU Ding-fa. The intermetallic formation in the extruded AlSi20/8009 aluminum alloy during annealing treatment [J]. Vacuum, 2019, 168: 108800.

[15] MULAZIMOGLU M H, ZALUSKA A, GRUZLESKI J E, PARAY F. Electron microscope study of Al−Fe−Si intermetallics in 6201 aluminum alloy [J]. Metallurgical and Materials Transactions A, 1996, 27: 929−936.

[16] TANIHATA H, SUGAWARA T, MATSUDA K, IKENO S. Effect of casting and homogenizing treatment conditions on the formation of Al−Fe−Si intermetallic compounds in 6063 Al−Mg−Si alloys [J]. Journal of Materials Science, 1999, 34: 1205−1210.

[17] KRENDELSBERGER N, WEITZER F, SCHUSTER J C. On the reaction scheme and liquidus surface in the ternary system Al−Fe−Si [J]. Metallurgical and Materials Transactions A, 2007, 38: 1681−1691.

[18] CHEN H L, CHEN Q, DU Y, BRATBERG J, ENGSTRÖM A. Update of Al−Fe−Si, Al−Mn−Si and Al−Fe−Mn−Si thermodynamic descriptions [J]. Transactions of Nonferrous Metals Society of China, 2014, 24: 2041−2053.

[19] KUIJPERS N C W, VERMOLEN F J, VUIK C, KOENIS P T G, NILSEN K E, van der ZWAAG S. The dependence of the β-AlFeSi to α-Al(FeMn)Si transformation kinetics in Al−Mg−Si alloys on the alloying elements [J]. Materials Science and Engineering A, 2005, 394: 9−19.

[20] CHENG Wei-jin, WANG Chaur-jeng. Effect of silicon on the formation of intermetallic phases in aluminide coating on mild steel [J]. Intermetallics, 2011, 19: 1455−1460.

[21] ZHANG Yu-bo, JIE Jin-chuan, GAO Yuan, LU Yi-ping, LI Ting-ju. Effects of ultrasonic treatment on the formation of iron-containing intermetallic compounds in Al−12%Si−2%Fe alloys [J]. Intermetallics, 2013, 42: 120−125.

[22] CASTRO-ROMÁN M J, AGUILERA-LUNA I, GAONA-CORONADO A A, HERRERA-TREJO M, TORRES-TORRES J. Role of Fe/Mn ratio and cooling rate on precipitation of iron intermetallics α-AlFeMnSi and β-AlFeSi in a 356 alloy [J]. Transactions of the Indian Institute Metals, 2015, 68: 1193−1197.

[23] YANG Wen-chao, GAO Feng, JI Shou-xun. Formation and sedimentation of Fe-rich intermetallics in Al−Si−Cu−Fe alloy [J]. Transactions of Nonferrous Metals Society of China, 2015, 25: 1704−1714.

[24] BELMARES-PERALES S, CASTRO-ROMÁN M, HERRERA-TREJO M, RAMÍREZ-VIDAURRI L E. Effect of cooling rate and Fe/Mn weight ratio on volume fractions of α-AlFeSi and β-AlFeSi phases in Al−7.3Si−3.5Cu alloy [J]. Metals and Materials International, 2008, 14: 307−314.

[25] VERMA A, KUMAR S, GRANT P S, O'REILLY K A Q. Influence of cooling rate on the Fe intermetallic formation in an AA6063 Al alloy [J]. Journal of Alloys and Compounds, 2013, 555: 274−282.

AlSi20/8009 铝合金在加热至熔点附近温度和冷却过程中的相演变

刘海彬[1]，苏华光[2]，傅定发[1]，蒋福林[1]，张 辉[1]

1. 湖南大学 材料科学与工程学院，长沙 410082；
2. 上海电缆研究所有限公司，上海 200093

摘 要：将 AlSi20/8009 铝合金加热至熔点附近温度后进行冷却，利用差热扫描量热仪、扫描电子显微镜、能量分散谱仪和 X 射线衍射仪研究外加 Si 对 $Al_{12}(Fe,V)_3Si$ 弥散体相演变的影响。结果发现，当 AlSi20/8009 铝合金在 580~600 °C 保温时，$Al_{12}(Fe,V)_3Si$ 和 Si 相演变成为针状 $Al_{4.5}FeSi$ 相和富 V 纳米相。提高保温温度至 620~640 °C，$Al_{4.5}FeSi$ 相和纳米相逆向演变为 $Al_{12}(Fe,V)_3Si$ 相和 Si 相，其中 $Al_{12}(Fe,V)_3Si$ 相具有粗大六边形形貌。当 AlSi20/8009 铝合金在 640 °C 保温后冷却至 570 °C 或更低的温度时，Si 相和粗大六边形 $Al_{12}(Fe,V)_3Si$ 相演变成片状 $Al_{4.5}FeSi$ 相和富 V 纳米相，这是一种不同于 Al−Fe−Si 三元体系的 $Al_{4.5}FeSi$ 相的新型形成路径。

关键词：SiC_p/8009 铝合金复合材料；相演变；冶金结合；重熔；冷却

(Edited by Wei-ping CHEN)